SUPPLEMENTARY INFORMATION, Text S1

PI3K-dependent crosstalk interactions converge with Ras as quantifiable inputs integrated by Erk

Chun-Chao Wang, Murat Cirit, and Jason M. Haugh

I. Kinetic Model

I.A. Receptor and PI3K Activation

I.A.1 PDGF Receptor Binding/Dimerization/Trafficking

The starting point for the kinetic model of the PDGF receptor signaling network was our previous model of receptor and PI3K activation, which was validated by quantitative experiments in the same cells as used here (Park et al, 2003; Schneider and Haugh, 2005). Definitions and base values of the relevant rate constants are listed in Table S1. Defining R, C_1, and C_2 as the density of free receptors, 1:1 receptor-ligand complexes, and functional receptor dimers in the membrane, respectively, and $[L]$ as the concentration of ligand (PDGF) added at time $t = 0$,

$$C_1 = [L]R/K_{D,L};$$

$$\frac{d(R + C_1)}{dt} = V_s - k_t(R + C_1) + 2\left(k_{-x}C_2 - k_x C_1^{\,2}\right);$$

$$\frac{dC_2}{dt} = k_x C_1^{\,2} - (k_{-x} + k_e)C_2;$$

$$R(0) + C_1(0) = R_0 = V_s/k_t; \quad C_2(0) = 0.$$

Here, $K_{D,L}$ is the dissociation constant characterizing 1:1 complex formation (fast on-off kinetics), V_s is the receptor insertion rate, and the rate constants k_x, k_{-x}, k_t, and k_e characterize receptor dimerization, dimer uncoupling, constitutive membrane turnover, and induced endocytosis of receptor dimers, respectively. Receptor densities are nondimensionalized by scaling R, C_1, C_2, and V_s by the initial surface receptor expression level, R_0; substituting its definition from above and simplifying,

$$\frac{dr}{dt} = \left(1 + \frac{[L]}{K_{D,L}}\right)^{-1}\left[k_t(1 - r - c_1) + 2\left(k_{-x}c_2 - k_x R_0 c_1^{\,2}\right)\right]; \quad \text{(Eq. S1)}$$

$$c_1 = [L]r/K_{D,L}; \quad r(0) + c_1(0) = 1; \qquad \text{(Eq. S2)}$$

$$\frac{dc_2}{dt} = k_x R_0 c_1^{\,2} - (k_{-x} + k_e)c_2; \quad c_2(0) = 0. \qquad \text{(Eq. S3)}$$

The output of this model is the fraction of receptors in dimers as a function of time, given by $2c_2(t)$. The parameter values were taken from the papers cited above, except for the basal receptor turnover rate constant k_t.

I.A.2 PI3K Recruitment and 3' PI Accumulation

We next present a model of PI3K recruitment and 3' PI production. In keeping with the notation used previously (Schneider and Haugh, 2005; Haugh, 2006), we refer to the fraction of the PI3K enzyme recruited as e_{PI3K}, and the dimensionless 3' PI messenger density is given by m_{3PI}. The rate of 3' PI accumulation in response to PDGF in fibroblasts is limited by 3' PI turnover, not the recruitment of PI3K (Park et al, 2003; Schneider and Haugh, 2004). Hence, it is justified to assume pseudo-equilibrium for PI3K binding:

$$e_{PI3K}(t) = \frac{\left[2\alpha_{PI3K}c_2(t) - e_{PI3K}(t)\right]\left[1 - e_{PI3K}(t)\right]}{\kappa_{PI3K}};$$

$$\alpha_{PI3K} = A_{mem}R_0 / E_{PI3K,Tot}; \quad \kappa_{PI3K} = V_{cyt}K_{D,PI3K} / E_{PI3K,Tot}.$$

The dimensionless parameters α_{PI3K} and κ_{PI3K} are cast in terms of A_{mem}, the surface area of the plasma membrane, $E_{PI3K,Tot}$, the total number of PI3K molecules per cell, V_{cyt}, the volume of the cytosol, and $K_{D,PI3K}$, the equilibrium dissociation constant for the receptor/PI3K interaction. The equation above is rearranged to obtain

$$e_{PI3K}(t) = \frac{1 + \kappa_{PI3K} + 2\alpha_{PI3K}c_2(t) - \sqrt{\left(1 + \kappa_{PI3K} + 2\alpha_{PI3K}c_2(t)\right)^2 - 8\alpha_{PI3K}c_2(t)}}{2}; \qquad \text{(Eq. S4)}$$

The stimulated accumulation of 3' PI lipids, with the normal basal level subtracted, is modeled in dimensionless form as follows (Park et al, 2003; Schneider and Haugh, 2005; Haugh, 2006):

$$\frac{dm_{3PI}}{dt} = k_{3PI}\left(e_{PI3K} - m_{3PI}\right); \quad m_{3PI}(0) = 0. \qquad \text{(Eq. S5)}$$

The base values of the parameters for this portion of the model (α_{PI3K}, κ_{PI3K}, and k_{3PI}), listed in Table S1, were assigned values that are quantitatively consistent with the data in our previous papers on PI3K signaling and hence were not subject to parameter fitting based on the new data presented in this paper.

Parameter	***Description***	***Value***
$K_{D,L}$	PDGF single-site dissociation constant	1.5 nM
k_xR_0	Dimerization rate constant	0.3 min^{-1}
k_{-x}	Dimer uncoupling rate constant	0.07 min^{-1}
k_e	Dimer endocytosis rate constant	0.2 min^{-1}
k_t	Basal receptor turnover rate constant	0.005 min^{-1}
α_{PI3K}	Receptor/PI3K expression ratio	80
κ_{PI3K}	Dimensionless receptor-PI3K dissociation constant	0.3
k_{3PI}	3' PI turnover rate constant	1.0 min^{-1}

Table S1: Kinetic model parameter definitions and values, PDGF receptor/PI3K module.

I.B. Ras/Erk Pathway

Based on our Ras-GTP and phospho-Erk data, the model at least needs to include the following processes: (*i*) recruitment of Ras-guanine nucleotide exchange factor (GEF) activity from the cytoplasm, controlled by the densities of activated receptors and 3' PI, mediating an increase in Ras-GTP level; (*ii*) activation of Raf and other MEK kinases, controlled by the densities of Ras-GTP and 3' PI; (*iii*) dual phosphorylation/dephosphorylation of MEK and of Erk; and (*iv*) negative feedback loops mediated by Erk affecting desensitization of GEF recruitment and up-regulation of MKP-1 expression. These aspects of the model are discussed below. Most of the Ras/Erk pathway parameters were estimated using a Monte-Carlo algorithm, described in detail in Part II of this Supplement. This strategy does not identify a "best-fit" value for each parameter but rather an ensemble of parameter sets that fit the data almost equally well. Definitions of the kinetic parameters and statistics concerning their estimation are summarized in Table S2.

I.B.1 GEF Recruitment and Ras-GTP Accumulation

For simplicity we do not model explicitly the various adaptor proteins involved in PDGF receptor-mediated Ras-GEF recruitment, such as Grb2, Shc, and Gab-1. Fractional GEF recruitment, $e_{GEF}(t)$, is assumed to respond rapidly to changes in the density of receptor dimers, $c_2(t)$, and 3' PI lipids, $m_{3PI}(t)$, according to the following approximate equilibrium-binding relation.

$$e_{GEF}(t) = \left[K_{GR}c_2(t) + K_{GP}m_{3PI}(t)\right]\left[f_{GEF}(t) - e_{GEF}(t)\right].$$

Other functions of c_2 and m_{3PI} on the right-hand side of this equation were evaluated (e.g., adding a dependence on the product of c_2 and m_{3PI}); not surprisingly, the nature of the experimental data does not adequately constrain the model to the extent that significant deviations from the assumed linear model are favored. Rearranging,

$$e_{GEF}(t) = \left[\frac{K_{GR}c_2(t) + K_{GP}m_{3PI}(t)}{1 + K_{GR}c_2(t) + K_{GP}m_{3PI}(t)}\right] f_{GEF}(t). \qquad \text{(Eq. S6)}$$

The dimensionless affinity parameter K_{GR} (GEF/Receptor) is analogous to the parameter grouping $2\alpha_{PI3K}/(1+\kappa_{PI3K})$ for receptor-mediated PI3K recruitment, described under section I.A.2. The model considers that 3' PI lipids might present or recruit independent binding sites for GEF, characterized by the dimensionless affinity constant K_{GP} (GEF/Phosphoinositide). The final component of the GEF recruitment model is the function $f_{GEF}(t)$, representing the fraction of the intracellular GEF available for recruitment, which is subject to feedback from MEK/Erk (section I.B.3).

The modeling of Ras-GTP accumulation is treated as in past models (Haugh and Lauffenburger, 1997; Haugh, 2002). Defining $M_{Ras\text{-}GTP}$ and $M_{Ras,Tot}$ as the area densities of membrane-associated Ras-GTP and total Ras (GTP- and GDP-bound), respectively,

$$\frac{dM_{Ras-GTP}}{dt} = \left(k_0 + k_{GEF}e_{GEF}\right)\left(M_{Ras,Tot} - M_{Ras-GTP}\right) - k_{GAP}M_{Ras-GTP}.$$

The rate constants k_0, k_{GEF}, and k_{GAP} characterize basal GDP/GTP exchange, maximal receptor-mediated activation of GEF activity, and GTP hydrolysis catalyzed by GTPase-accelerating proteins (GAPs), respectively. We define the dimensionless $m_{Ras}(t)$ by analogy to $m_{3PI}(t)$ in that

$m_{Ras} = 0$ when $e_{GEF} = 0$ (representing the basal state) and $m_{Ras} = 1$ when $e_{GEF} = 1$. Manipulation of the equation above gives

$$\frac{dm_{Ras}}{dt} = k_{Ras}\left[(1+\Gamma)e_{GEF} - (1+\Gamma e_{GEF})m_{Ras}\right]; \quad m_{Ras}(0) = 0; \qquad \text{(Eq. S7)}$$
$$k_{Ras} = k_0 + k_{GAP}; \quad \Gamma = k_{GEF}/k_{Ras}.$$

In this particular model, we do not consider receptor-mediated activation of GTPase-accelerating protein (GAP) activity, but at least in rough terms one could in any case consider the gain parameter Γ to represent the ratio of GEF/GAP activities under maximal stimulation conditions.

This portion of the model was parameterized as follows. Based on previous experiments (Kaur et al, 2006), it is known that only a small fraction of Ras in our cells is converted to the GTP-bound form, consistent with $\Gamma << 1$ and $m_{Ras} \approx e_{GEF}$ at steady state; hence, $\Gamma = 0.1$ was chosen as an arbitrary, order-of-magnitude estimate. Ras-GTP levels peak at t ~ 3 minutes or earlier, and the temporal resolution of our kinetic data does not allow for accurate estimation of the effective rate constant k_{Ras}. A sufficiently high value of 1 min^{-1} was therefore assigned. The values of the 2 parameters characterizing GEF recruitment (K_{GR}, K_{GP}) were subject to our parameter estimation algorithm.

I.B.2 Ras- and PI3K-dependent Activation of the Erk cascade

Ras and PI3K are responsible for activating serine-threonine kinases that activate MEK, which in turn activates Erk. There are multiple isoforms of Raf (notably, Raf-1 and B-Raf) and also other MEK kinases (e.g., Pak, PDK-1). In the minimal mathematical description, we identify and model two modes of activation at this level:

1. Mode 1 (x_1): Ras-dependent, PI3K-independent. This is the only mode leading to MEK/Erk activation in PI3K-inhibited cells.
2. Mode 2 (x_2): Ras-independent, PI3K-dependent. This accounts for MEK/Erk activation in S17N Ras-expressing cells.

The dimensionless variables x_1 and x_2 are assumed to be independent; that is, they represent either distinct enzymes or activation of the same enzyme with most of it remaining in the inactive state. We also analyzed a more complex model containing an additional MEK kinase activity, x_3, which was both Ras- and PI3K-dependent. In that case, the algorithm generally chose parameters so as to marginalize the influence of x_3 downstream; hence, we removed this pathway from the model.

MEK and Erk are successively activated via dual phosphorylation mechanisms that are thought to be distributive (nonprocessive); i.e., MEK must be engaged by a MEK kinase in separate encounters to be phosphorylated on its two activation sites, and likewise for Erk phosphorylation by MEK. The dual phosphorylation mechanism has interesting theoretical properties that have been characterized by other groups over the years (Ferrell, 1996; Ferrell, 2002; Markevich et al, 2004; Wang et al, 2006; Qiao et al, 2007), and so we wish to maintain that character without sacrificing model simplicity (in terms of the number of adjustable parameters). We define y, y_p, and y_{pp} as the fractions of MEK that are unphosphorylated, mono-phosphorylated, and dually phosphorylated, respectively, and z, z_p, and z_{pp} as the corresponding fractions of Erk. There are also phosphatases, *yph* and *zph*, which dephosphorylate MEK and Erk, respectively.

Our model assumes quasi-steady state for the enzyme-substrate complexes (Michaelis-Menten kinetics). A notable assumption here is that the substrates are in excess relative to the enzymes; it is fully recognized that this assumption might not be strictly satisfied inside the cell, and this aspect of the model can be refined as additional data come to light. We do allow competition for common enzymes; unphosphorylated and mono-phosphorylated forms of MEK and Erk compete with each other for the upstream kinase, and the phosphorylated forms compete with each other for binding to the corresponding phosphatase. Further, active MEK kinase can be saturated by inactive MEK so as to reduce the rate of MEK kinase dephosphorylation, and saturation of active MEK by inactive Erk reduces the rate of MEK dephosphorylation. The quasi-steady state expressions for the enzyme-substrate complexes, denoted by (enzyme • substrate), are as follows.

$$(x_1 \bullet y) \approx \frac{(x_1)_{free}(y)_{free}}{\tilde{K}_{M,x11}} \approx \frac{(x_1)_{free}\, y}{\tilde{K}_{M,x11}}; \quad (x_1 \bullet y_p) \approx \frac{(x_1)_{free}(y_p)_{free}}{\tilde{K}_{M,x12}} \approx \frac{(x_1)_{free}\, y_p}{\tilde{K}_{M,x12}};$$

$$(x_1)_{free} \approx \frac{x_1}{1 + y/\tilde{K}_{M,x11} + y_p/\tilde{K}_{M,x12}};$$

$$(x_2 \bullet y) \approx \frac{(x_2)_{free}(y)_{free}}{\tilde{K}_{M,x21}} \approx \frac{(x_2)_{free}\, y}{\tilde{K}_{M,x21}}; \quad (x_2 \bullet y_p) \approx \frac{(x_1)_{free}(y_p)_{free}}{\tilde{K}_{M,x12}} \approx \frac{(x_1)_{free}\, y_p}{\tilde{K}_{M,x12}};$$

$$(x_2)_{free} \approx \frac{x_2}{1 + y/\tilde{K}_{M,x21} + y_p/\tilde{K}_{M,x22}};$$

$$(y_{pp} \bullet z) \approx \frac{(y_{pp})_{free}(z)_{free}}{\tilde{K}_{M,y1}} \approx \frac{(y_{pp})_{free}\, z}{\tilde{K}_{M,y1}}; \quad (y_{pp} \bullet z_p) \approx \frac{(y_{pp})_{free}(z_p)_{free}}{\tilde{K}_{M,y2}} \approx \frac{(y_{pp})_{free}\, z_p}{\tilde{K}_{M,y2}};$$

$$(y_{pp})_{free} \approx \frac{y_{pp}}{1 + z/\tilde{K}_{M,y1} + z_p/\tilde{K}_{M,y2}};$$

$$(yph \bullet y_p) \approx \frac{(yph)_{free}(y_p)_{free}}{\tilde{K}_{M,yph1}} \approx \frac{(yph)_{free}\, y_p}{\tilde{K}_{M,yph1}};$$

$$(yph \bullet y_{pp}) \approx \frac{(yph)_{free}(y_{pp})_{free}}{\tilde{K}_{M,yph2}} \approx \frac{(yph)_{free}\, y_{pp}/\tilde{K}_{M,yph2}}{1 + z/\tilde{K}_{M,y1} + z_p/\tilde{K}_{M,y2}};$$

$$(yph)_{free} \approx \frac{yph\left(1 + z/\tilde{K}_{M,y1} + z_p/\tilde{K}_{M,y2}\right)}{\left(1 + z/\tilde{K}_{M,y1} + z_p/\tilde{K}_{M,y2}\right)\left(1 + y_p/\tilde{K}_{M,yph1}\right) + y_{pp}/\tilde{K}_{M,yph2}};$$

$$(zph \bullet z_p) \approx \frac{(zph)_{free}(z_p)_{free}}{\tilde{K}_{M,zph1}} \approx \frac{(zph)_{free}\, z_p}{\tilde{K}_{M,zph1}}; \quad (zph \bullet z_{pp}) \approx \frac{(zph)_{free}(z_{pp})_{free}}{\tilde{K}_{M,yph2}} \approx \frac{(zph)_{free}\, z_{pp}}{\tilde{K}_{M,yph2}};$$

$$(zph)_{free} \approx \frac{zph}{1 + z_p/\tilde{K}_{M,zph1} + z_{pp}/\tilde{K}_{M,zph2}}.$$

The dimensionless parameters $\tilde{K}_{M,xi1}$ and $\tilde{K}_{M,xi2}$ are Michaelis constants, scaled by the total MEK concentration, characterizing the first and second phosphorylations of MEK by enzyme x_i; $\tilde{K}_{M,y1}$ and $\tilde{K}_{M,y2}$ are the corresponding Michaelis constants for Erk phosphorylation by active MEK,

$\tilde{K}_{M,yph1}$ and $\tilde{K}_{M,yph2}$ are the corresponding Michaelis constants for MEK dephosphorylation, and $\tilde{K}_{M,zph1}$ and $\tilde{K}_{M,zph2}$ are the corresponding Michaelis constants for Erk dephosphorylation.

The conservation equations for the MEK kinases assume that these enzymes are mostly maintained in their inactive states, and that their deactivation is far from saturation (pseudo-first order). As noted above, however, we account for the potential saturation of each active MEK kinase by inactive MEK. It is noted that the PI3K-dependent mechanism could rightly be modeled as a sequence of two or more steps, because unlike Ras-GTP, 3' PIs are probably not capable of directly interacting with the MEK kinase(s) (with the exception of PDK-1). To reduce the number of parameters, we lump these processes into a single, rate-limiting step for x_2; however, we allow for partial saturation of this mechanism with respect to the 3' PI level, by including a saturation parameter, K_{x2}. Cast in terms of dimensionless concentrations, the rate equations for the MEK kinases are

$$\frac{dx_1}{dt} = k_{d,x1}\left(m_{Ras} - \frac{x_1}{1 + y/\tilde{K}_{M,x11} + y_p/\tilde{K}_{M,x12}}\right); \quad x_1(0) = 0; \qquad \text{(Eq. S8)}$$

$$\frac{dx_2}{dt} = k_{d,x2}\left[\frac{(1+K_{x2})m_{3PI}}{1+K_{x2}m_{3PI}} - \frac{x_2}{1 + y/\tilde{K}_{M,x21} + y_p/\tilde{K}_{M,x22}}\right]; \quad x_2(0) = 0; \quad \text{(Eq. S9)}$$

For MEK, the conservation equations are

$$\frac{dy}{dt} = -\sum_{i=1}^{2}\frac{\tilde{V}_{\max,xi1}x_i\, y/\tilde{K}_{M,xi1}}{1 + y/\tilde{K}_{M,xi1} + y_p/\tilde{K}_{M,xi2}} + \frac{\tilde{V}_{\max,yph1}\, y_p/\tilde{K}_{M,yph1}}{1 + y_p/\tilde{K}_{M,yph1} + y_{pp}/\tilde{K}_{M,yph2}}; \quad y(0) = 1; \qquad \text{(Eq. S10)}$$

$$\frac{dy_{pp}}{dt} = \sum_{i=1}^{2}\frac{\tilde{V}_{\max,xi2}x_i\, y_p/\tilde{K}_{M,xi2}}{1 + y/\tilde{K}_{M,xi1} + y_p/\tilde{K}_{M,xi2}} - \frac{\tilde{V}_{\max,yph2}\, y_{pp}/\tilde{K}_{M,yph2}}{\left(1 + z/\tilde{K}_{M,y1} + z_p/\tilde{K}_{M,y2}\right)\left(1 + y_p/\tilde{K}_{M,yph1}\right) + y_{pp}/\tilde{K}_{M,yph2}}; \quad y_{pp}(0) = 0; \qquad \text{(Eq. S11)}$$

$$y_p = 1 - y - y_{pp}. \qquad \text{(Eq. S12)}$$

As shown in Eqs. S10 & S11, the model allows x_1 and x_2 to possess distinct catalytic properties with respect to MEK phosphorylation. The parameters $\tilde{V}_{\max,xi1}$ and $\tilde{V}_{\max,xi2}$ account for the abundance of the *i*th MEK kinase mode at maximal stimulation as well as its k_{cat} values for the first and second phosphorylations of MEK, respectively. They are scaled by the total concentration of MEK and therefore have units of inverse time. Corresponding parameters are specified for the single MEK phosphatase (*yph*), which is assumed to have constant abundance, and for Erk phosphorylation/dephosphorylation. The rate expressions for Erk phosphorylation are

$$\frac{dz}{dt} = -\frac{\tilde{V}_{\max,y1}y_{pp}\, z/\tilde{K}_{M,y1}}{1 + z/\tilde{K}_{M,y1} + z_p/\tilde{K}_{M,y2}} + \frac{\tilde{V}_{\max,zph1}e_{ph}\, z_p/\tilde{K}_{M,zph1}}{1 + z_p/\tilde{K}_{M,zph1} + z_{pp}/\tilde{K}_{M,zph2}}; \quad z(0) = 1; \qquad \text{(Eq. S13)}$$

$$\frac{dz_{pp}}{dt} = \frac{\tilde{V}_{\max,y2}y_{pp}\, z_p/\tilde{K}_{M,y2}}{1 + z/\tilde{K}_{M,y1} + z_p/\tilde{K}_{M,y2}} - \frac{\tilde{V}_{\max,zph2}e_{ph}\, z_{pp}/\tilde{K}_{M,zph2}}{1 + z_p/\tilde{K}_{M,zph1} + z_{pp}/\tilde{K}_{M,zph2}}; \quad z_{pp}(0) = 0 \qquad \text{(Eq. S14)}$$

$$z_p = 1 - z - z_{pp}. \qquad \text{(Eq. S15)}$$

The function $e_{ph}(t)$ represents the dimensionless abundance of the dual-specificity phosphatase that dephosphorylates Erk and thus counteracts active MEK; this phosphatase is subject to up-regulation through a MAPK-dependent negative feedback loop (section I.B.3 below).

Even with a fair number of parameter-reducing simplifications, modeling the Erk cascade introduces a relatively large number of adjustable rate constants (23). This number may be reduced if one or more of the enzymes can be assumed to operate far from saturation ($\tilde{K}_M$ values >> 1).

I.B.3 Negative Feedback Loops Eliciting GEF Desensitization and Up-regulation of MKP-1

These negative feedback loops are embodied by the functions $f_{GEF}(t)$ and $e_{ph}(t)$, as introduced in sections I.B.1 and I.B.2, respectively. GEF desensitization, which involves Erk-dependent hyperphosphorylation, affects the fraction of GEF available, $f_{GEF}(t)$.

$$\frac{df_{GEF}}{dt} = -k_{FB,f}\left[\frac{{z_{pp}}^n}{{Z_f}^n + {z_{pp}}^n} f_{GEF} - \frac{1}{K_f}\left(1 - f_{GEF}\right)\right]; \quad f_{GEF}(0) = 1; \qquad \text{(Eq. S16)}$$

This expression allows for potentially switch-like or a more graded transition (Hill coefficient $n \geq 1$) as well as fast or slow "reset" kinetics. As shown in Table 2, one could set $n = 1$ without affecting the model output significantly. The rate constant $k_{FB,f}$ defines the time scale associated with the feedback loop, and K_f defines its gain (maximum ratio of desensitization and reset frequencies).

For e_{ph}, the model needs to account for the observation that MKP-1 appears with a delay of ~ 15 minutes. Thus, we impose a variable w, possibly representing a transcription factor activity, which builds up slowly and switches on MKP-1 expression.

$$\frac{dw}{dt} = k_{d,w}\left(z_{pp} - w\right); \quad w(0) = 0; \qquad \text{(Eq. S17)}$$

$$\frac{de_{ph}}{dt} = k_{FB,ph}\left[\frac{w^p}{{W_{ph}}^p + w^p} - \frac{1}{K_{ph}}\left(e_{ph} - 1\right)\right]; \quad e_{ph}(0) = 1. \qquad \text{(Eq. S18)}$$

These two Erk-dependent feedback loops introduce 9 additional parameters.

I.C. Modeling Molecular Perturbations Affecting Erk Phosphorylation

PI3K inhibition is modeled by setting $m_{3PI} = 0$, which affects the Ras/Erk pathway both upstream and downstream of Ras. MEK inhibition, which affects Ras-GEF desensitization, is modeled by setting $f_{GEF} = 1$. S17N Ras is modeled by setting $m_{Ras} = 0$. Chronic activation by phorbol ester is modeled by assuming that MEK activation is saturated (y_{pp} set to 1).

Parameter	*Description*	*Minimum*	*Lower Quartile*	*Median*	*Upper Quartile*	*Maximum*
K_{GR}	Affinity constant, GEF/receptor binding	102	394	495	640	1730
K_{GP}	Affinity constant, 3' PI-dependent GEF binding	0.00266	3.47	5.09	6.51	32.7
k_{Ras}	Characteristic rate constant, Ras-GTP loading			1/min *		
Γ	Maximally stimulated GEF/GAP activity ratio			0.1 *		
$k_{d,x1}$	MEK kinase deactivation rate constant (Ras-activated)	0.203/min	0.561/min	0.745/min	1.21/min	12.9/min
$k_{d,x2}$	MEK kinase deactivation rate constant (PI3K-activated)	0.305/min	1.77/min	2.85/min	11.2/min	282/min
K_{x2}	Saturation constant, PI3K-dependent MEK kinase activation	0.251	5.25	6.77	10.2	31.0
$\tilde{V}_{\max,x11}/\tilde{K}_{M,x11}$	Cat. efficiency, MEK --> pMEK (Ras-activated)	0.0579/min	0.516/min	1.18/min	1.62/min	71.3/min
$\tilde{K}_{M,x11}$	Mich. constant, MEK --> pMEK (Ras-activated)	0.343	20.1	30.3	250	2570
$\tilde{V}_{\max,x21}/\tilde{K}_{M,x21}$	Cat. efficiency, MEK --> pMEK (PI3K-activated)	0.0302/min	0.236/min	0.405/min	0.907/min	353/min
$\tilde{K}_{M,x21}$	Mich. constant, MEK --> pMEK (PI3K-activated)	0.0568	13.7	21.6	203	3710
$\tilde{V}_{\max,yph1}/\tilde{K}_{M,yph1}$	Catalytic efficiency, pMEK --> MEK	$5.6\text{x}10^{-4}$/min	1.65/min	4.40/min	14.7/min	483/min
$\tilde{K}_{M,yph1}$	Michaelis constant, pMEK --> MEK	0.573	23.0	44.0	97.8	445
$\tilde{V}_{\max,x12}/\tilde{K}_{M,x12}$	Cat. efficiency, pMEK --> ppMEK (Ras-activated)	0.115/min	3.54/min	4.71/min	15.5/min	146/min
$\tilde{K}_{M,x12}$	Mich. constant, pMEK --> ppMEK (Ras-activated)	2.81	18.6	45.5	114	758
$\tilde{V}_{\max,x22}/\tilde{K}_{M,x22}$	Cat. efficiency, pMEK --> ppMEK (PI3K-activated)	0.0318/min	1.09/min	2.41/min	9.45/min	77.6/min
$\tilde{K}_{M,x22}$	Mich. constant, pMEK --> ppMEK (PI3K-activated)	0.876	9.59	15.7	31.6	878
$\tilde{V}_{\max,yph2}/\tilde{K}_{M,yph2}$	Catalytic efficiency, ppMEK --> pMEK	0.233/min	4.20/min	6.77/min	9.07/min	52.2/min
$\tilde{K}_{M,yph2}$	Michaelis constant, ppMEK --> pMEK	1.05	7.99	12.7	42.5	254
$\tilde{V}_{\max,y1}/\tilde{K}_{M,y1}$	Catalytic efficiency, Erk --> pErk	0.862/min	6.57/min	11.8/min	52.8/min	$> 10^4$/min
$\tilde{K}_{M,y1}$	Michaelis constant, Erk --> pErk	0.0146	9.91	31.9	45.5	890
$\tilde{V}_{\max,zph1}/\tilde{K}_{M,zph1}$	Catalytic efficiency, pErk --> Erk	$1.1\text{x}10^{-4}$/min	0.167/min	0.451/min	1.11/min	63.2/min
$\tilde{K}_{M,zph1}$	Michaelis constant, pErk --> Erk	0.275	8.27	14.0	37.0	167

$\tilde{V}_{\max y2}/\tilde{K}_{M\,y2}$	Catalytic efficiency, pErk --> ppErk	0.669/min	8.16/min	31.9/min	66.9/min	7730/min
$\tilde{K}_{M\,y2}$	Michaelis constant, pErk --> ppErk	0.0481	4.21	8.81	80.7	944
$\tilde{V}_{\max zph2}/\tilde{K}_{M\,zph2}$	Catalytic efficiency, ppErk --> pErk	0.0263/min	0.122/min	0.228/min	0.493/min	13.7/min
$\tilde{K}_{M\,zph2}$	Michaelis constant, ppErk --> pErk	1.10	9.98	31.5	195	797
$k_{FB,f}$	Feedback rate constant, GEF desensitization	0.104/min	0.763/min	0.976/min	1.56/min	23.7/min
Z_f	Dimensionless threshold, GEF desensitization	0.00829	0.146	0.272	0.507	2.50
n	Hill coefficient, GEF densensitization	1.00 †	1.02	1.03	1.05	1.48
K_f	Gain coefficient, GEF desensitization	1.04	3.16	3.76	5.17	16.6
k_w	Delay rate constant, MKP up-regulation	0.00646/min	0.0187/min	0.0333/min	0.0914/min	0.478/min
$k_{FB,ph}$	Feedback rate constant, MKP up-regulation	0.0375/min	0.998/min	2.34/min	3.69/min	60.6/min
W_{ph}	Dimensionless threshold, MKP up-regulation	0.107	0.248	0.385	1.11	12.3
p	Hill coefficient, MKP up-regulation	1.10 †	1.76	1.98	2.56	24.7
K_{ph}	Gain coefficient, MKP up-regulation	1.35	3.08	4.64	25.1	8055

Table S2: Kinetic model parameters, Ras/Erk pathway module. A Monte-Carlo algorithm was used to estimate all but two of these parameter values, producing an ensemble of parameter sets that fit the data set almost equally well. See Part II of this Supplement for more details. * These two parameters were fixed. † The Hill coefficients n and p were constrained to be no lower than 1. Highlighted values are deemed arbitrarily high (yellow) or low (cyan).

II. Parameter Estimation

II.A. Metropolis Algorithm

II.A.1 Description of the Algorithm

The values of all but 2 of the 36 parameters listed in Table S2 were subject to a Monte Carlo estimation routine based on the Metropolis algorithm (Metropolis et al, 1953). The algorithm was implemented in MATLAB (MathWorks, Natick, MA), adapted from code provided by Tim Elston (Department of Pharmacology, UNC-Chapel Hill) (Violin et al, 2008). The following data sets were used to constrain the model: dually phosphorylated Erk under DMSO control, Ras-inhibited, and PI3K-inhibited conditions, Ras-GTP under control, PI3K-inhibited, and MEK-inhibited conditions, and MKP expression under control and Ras-inhibited conditions. In order to set all of the data on a similar scale, the mean of the normalized data values under control conditions, 1 nM PDGF stimulation, were set to 1. Later, the data presented in Supplementary Fig. S3 were incorporated to constrain the saturation level of ppErk (stimulated by phorbol ester); those data were aligned with the other ppErk data by minimizing the sum of the squared deviations between the corresponding time points in control cells stimulated with 1 nM PDGF.

The algorithm works as follows.

1) An initial set of parameters is chosen. For the exponents n and p (Table S2), which were constrained to be no less than 1, the corresponding parameter value in the algorithm was added to its lower limit (e.g., $n = 1 + x$).

2) The dimensionless model output is computed using the stiff solver ode15s.

3) The model outputs based on the current parameter set are modified by alignment factors to directly compare with data, one each for ppErk, Ras-GTP, and MKP expression. The values of these three factors, a_j, are chosen such that the sum of squared deviations (SSD) for each of the three data types j (ppErk, Ras-GTP, MKP-1), comparing measured and calculated values at each data point i,

$$SSD_j = \sum_i \left(y_{measured,ij} - a_j y_{model,ij} \right)^2 ,$$

is minimized. This step is done by systematically subdividing the range of possible values until each SSD_j can no longer be reduced by more than 0.1%. For example, for a dimensionless variable between 0 and 1 and corresponding data with a peak value greater than 1 in arbitrary units, we know that $a_j > 1$, in which case we know that $0 < 1/a_j < 1$. The minimum SSD values thus obtained are saved and used to evaluate the closeness of fit, as described in the following section.

4) A new set of parameters is determined from the old set as follows.

$$k_{i,new} = k_{i,old} \left(1 + \alpha \, \mathrm{randn} \right),$$

where k_i is one of the model parameters, and randn is a random number drawn for each parameter from a normal distribution centered on zero with $\sigma = 1$. Thus, α is a parameter of the algorithm that governs how much the parameter values tend to change between iterations. Its value affects the efficiency of the algorithm, and after extensive

experimentation we concluded that a value of $\alpha = 0.05$ is close to optimal for this application. That value was used throughout the analysis reported here. If any of the new parameters is below 10^{-4} or greater than 10^{4}, the new value is thrown out, and another value is drawn based on the old value.

5) Steps 2-4 are repeated using the new parameter set, and its SSD_j are evaluated. If defined criteria are satisfied (see section II.A.2 below), the new parameter set is accepted; otherwise, it is thrown out, and the previous set is used again.

6) The procedure is repeated until the desired number of accepted parameter sets is achieved. All of the accepted parameter sets are saved in a matrix for further analysis.

II.A.2 Generation of a Parameter Ensemble

The strategy for using the algorithm was as follows. First, we established a suitable initial parameter set. This was done by randomly varying the parameters as described above until a weighted sum of SSD values converged to a near-minimal value; in this exercise, it was confirmed that different starting guesses resulted in approximately the same value of the weighted SSD. Once a reference parameter set was established, it was used as the starting point for an extensive search of the parameter space, with the goal of collecting parameter sets that fit the data nearly as well as or better than the initial parameter set. A parameter set was selected if it produced a SSD value less than 1.5 for each of the following data subsets: ppErk with DMSO, ppErk in S17N Ras cells, ppErk in LY294002-treated cells, Ras-GTP measurements, MKP-1 measurements, and ppErk with DMSO or PMA. After some experimentation, it was found that an additional criterion was needed to ensure that the ppErk, S17N Ras data for the lowest PDGF concentration (30 pM) was fit adequately, and hence the parameter sets also had to have a SSD < 0.35 for those particular data points. Finally, to improve the quality of fit of the PI3K-inhibited ppErk data, the parameter sets obtained were sorted according to their SSD value for those data, and sets with SSD < 1.0 for that subset of data were selected. Statistics for this ensemble, representing 10,000 of the "best" parameter sets (out of > 60,000 initially chosen), are summarized in Table S2.

II.B. Ensemble Averaging and Analysis

With the ensemble of parameter sets saved as a matrix, MATLAB was used to recalculate the model output for each parameter set and store those values in a larger matrix. For each experimental condition and time point, an ensemble mean and standard deviation (n = 10,000) were computed, and these values were used to compare the model with the experimental data in Fig. 7. To predict the outcomes of certain perturbations, namely the inhibition of PI3K-dependent crosstalk to Ras-GEF or to MEK (Fig. 9), the corresponding changes in the parameter values ($K_{GP} = 0$ or $\tilde{V}_{\max,x21} = \tilde{V}_{\max,x22} = 0$, respectively) were made in each of the 10,000 parameter sets, and the mean and standard deviation of the model output were recomputed.

The analysis of MEK phosphorylation presented in Fig. 8A was carried out as follows. The maximum phosphorylation of MEK by pathway i (i = 1 for Ras-dependent, i = 2 for PI3K-dependent) on site j (j = 1 or 2) is characterized by the ratio of catalytic efficiencies,

$$C_{xij} = \frac{\tilde{V}_{\max,xij} / \tilde{K}_{M,xij}}{\tilde{V}_{\max,yphj} / \tilde{K}_{M,yphj}}.$$

Fig. 8A shows scatter plots of maximum PI3K-dependent phosphorylation of site 1 (C_{x21}) versus maximum Ras-dependent phosphorylation of site 1 (C_{x11}) and of maximum PI3K-dependent phosphorylation of site 2 (C_{x22}) versus maximum Ras-dependent phosphorylation of site 2 (C_{x12}), with each parameter set in the ensemble represented as a dot. The MEK activation comparator (MAC), referred to in the main text, incorporates the phosphorylation of both MEK sites and was calculated as follows. Suppose that the MEK kinases and phosphatase are far from saturation and that only one of the two MEK activation pathways is present and maximally activated (x_i = 1). If such a system were allowed to reach steady state, Eqs. S10-S12 reduce to

$$y_p = C_{xi1} y; \quad y_{pp} = C_{xi2} y_p;$$
$$y + y_p + y_{pp} = 1;$$
$$y_{pp} = \frac{\Psi_i}{1+\Psi_i}; \quad \Psi_i = \frac{C_{xi1} C_{xi2}}{1+C_{xi1}}.$$

The MAC ratio compares the capacity for activation of y_{pp} thus obtained for the PI3K-dependent pathway to that of the Ras-dependent pathway, according to

$$MAC = \frac{\Psi_2}{\Psi_1} = \left(\frac{C_{x21} C_{x22}}{1+C_{x21}}\right) \Big/ \left(\frac{C_{x11} C_{x12}}{1+C_{x11}}\right).$$

The impact of the negative feedback affecting Ras-GEF recruitment is assessed by reducing the values of C_{x11} and C_{x12} by the same factor.

The analysis of Ras-GEF recruitment presented in Fig. 8B was carried out as follows. It is apparent from Eq. S6 that GEF recruitment, as a fraction of the amount available, is determined by the magnitude of

$$K_{GR} c_2(t) + K_{GP} m_{3PI}(t)$$

A balanced comparison of the two terms in this sum, representing the PI3K-independent and PI3K-dependent GEF recruitment modes, is complicated by the fact that the dimensionless variables c_2 and m_{3PI} are normalized differently. However, in the limit of low PDGF concentrations (with $e_{PI3K} << 1$), m_{3PI} is proportional to c_2 at quasi-steady state (Eq. S4 & S5), with

$$m_{3PI} = e_{PI3K} \approx \frac{2\alpha_{PI3K}}{1+\kappa_{PI3K}} c_2 \qquad (e_{PI3K} << 1, \text{ quasi-steady state}).$$

For the parameters used here, the proportionality constant is equal to 123. Fig. 8B shows a scatter plot of PI3K-dependent GEF recruitment, expressed as the value of K_{GP}, versus the corresponding PI3K-independent GEF recruitment, expressed on a comparable scale as the value of K_{GR} divided by 123; each parameter set in the ensemble is represented as a dot. The GEF recruitment comparator (GRC) compares these contributions in terms of a ratio,

$$GRC = \left(\frac{2\alpha_{PI3K}}{1+\kappa_{PI3K}}\right) \frac{K_{GP}}{K_{GR}} = 123 \frac{K_{GP}}{K_{GR}}.$$

III. References

Ferrell JE, Jr. (1996) Tripping the switch fantastic: how a protein kinase cascade can convert graded inputs into switch-like outputs. *Trends Biochem Sci* **21:** 460-466

Ferrell JE, Jr. (2002) Self-perpetuating states in signal transduction: positive feedback, double-negative feedback and bistability. *Curr Opin Cell Biol* **14:** 140-148

Haugh JM (2002) A unified model for signal transduction reactions in cellular membranes. *Biophys J* **82:** 591-604

Haugh JM (2006) Deterministic model of dermal wound invasion incorporating receptor-mediated signal transduction and spatial gradient sensing. *Biophys J* **90:** 2297-2308

Haugh JM, Lauffenburger DA (1997) Physical modulation of intracellular signaling processes by locational regulation. *Biophys J* **72:** 2014-2031

Kaur H, Park CS, Lewis JM, Haugh JM (2006) Quantitative model of Ras/phosphoinositide 3-kinase signalling cross-talk based on co-operative molecular assembly. *Biochem J* **393:** 235-243

Markevich NI, Hoek JB, Kholodenko BN (2004) Signaling switches and bistability arising from multisite phosphorylation in protein kinase cascades. *J Cell Biol* **164:** 353-359

Metropolis N, Rosenbluth AW, Rosenbluth MN, Teller AH, Teller E (1953) Equation of state calculations by fast computing machines. *J Chem Phys* **21:** 1087-1092

Park CS, Schneider IC, Haugh JM (2003) Kinetic analysis of platelet-derived growth factor receptor/phosphoinositide 3-kinase/Akt signaling in fibroblasts. *J Biol Chem* **278:** 37064-37072

Qiao L, Nachbar RB, Kevrekidis IG, Shvartsman SY (2007) Bistability and oscillations in the Huang-Ferrell Model of MAPK signaling. *PLoS Comp Biol* **3:** e184

Schneider IC, Haugh JM (2004) Spatial analysis of 3' phosphoinositide signaling in living fibroblasts: II. Parameter estimates for individual cells from experiments. *Biophys J* **86:** 599-608

Schneider IC, Haugh JM (2005) Quantitative elucidation of a distinct spatial gradient-sensing mechanism in fibroblasts. *J Cell Biol* **171:** 883-892

Violin JD, Dipilato LM, Yildirim N, Elston TC, Zhang J, Lefkowitz RJ (2008) β2-adrenergic receptor signaling and desensitization elucidated by quantitative modeling of real time cAMP dynamics. *J Biol Chem* **283:** 2949-2961

Wang X, Hao N, Dohlman HG, Elston TC (2006) Bistability, stochasticity, and oscillations in the mitogen-activated protein kinase cascade. *Biophys J* **90:** 1961-1978

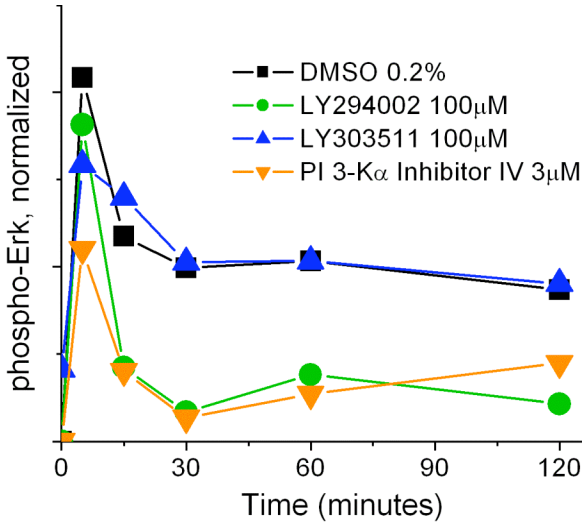

Figure S1. Specificity of PI3K inhibition. The PI3K inhibitor LY294002 is known to have off-target effects. LY303511 has the same or similar pharmacological profile with respect to those targets but does not inhibit PI3K. The results shown, representative of two independent experiments, confirm that LY303511 does not significantly affect Erk phosphorylation, stimulated by PDGF (1 nM) and quantified by immunoblotting (phospho-Erk/total Erk), and that another PI3K inhibitor yields similar effects as LY294002.

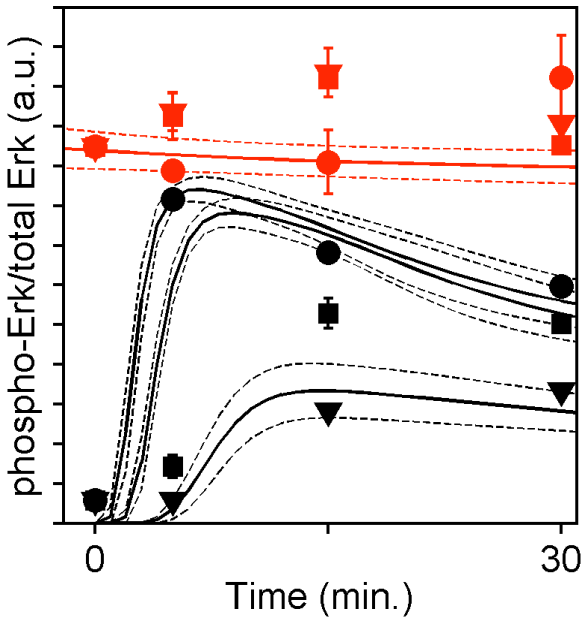

Figure S2. Saturation of the Erk cascade using phorbol ester. Cells were pretreated for 15 minutes with DMSO only (black symbols) or 200 nM PMA (red symbols), prior to stimulation with PDGF-BB: 30 pM (triangles), 100 pM (squares), or 1 nM (circles). Erk phosphorylation was determined in duplicate by quantitative immunoblotting (phospho-Erk/total Erk), and the values are expressed as mean ± s.e.m. (n = 2. The error bars are shown for illustrative purposes only; they are equivalent to the range divided by 1.41). The results indicate that Erk phosphorylation is close to saturation in PMA treated cells. In the cells not treated with PMA, the PDGF-stimulated response is 80-90% of the apparent saturation level. The solid curves represent the corresponding ensemble means for the kinetic model, and the dashed curves are mean ± s.d. (n = 10,000).

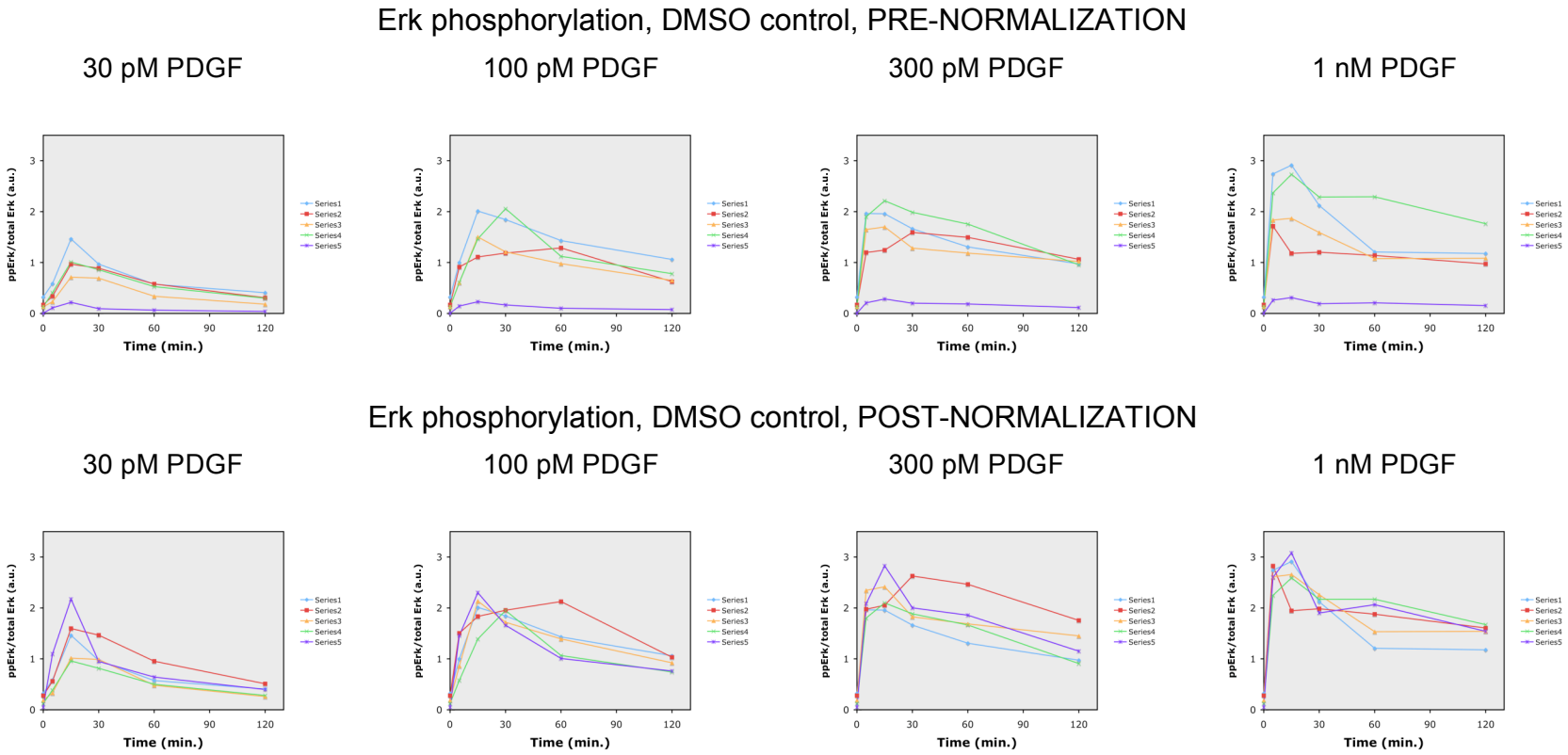

Figure S3. Data normalization for biological (day-to-day) variability. The normalization procedure described under Materials and Methods is demonstrated on the Erk phosphorylation data for the DMSO control, Fig. 1C&E. The top row shows the unaligned data (normalized already by total Erk). Different colors mark measured time courses from independent experiments. Note that, in this case, the Erk phosphorylation values from one of the experiments (Series 5) are much lower than the rest. The bottom row shows the data after our normalization protocol. The values from each day of experiments are multiplied by a scaling factor so as to minimize the average coefficient of variation for the control, 1 nM PDGF time course. Those scaling factors are applied to the lower PDGF concentrations shown here and also the rest of the lysates collected on the same day (in this case, from cells treated with LY294002 and from cells treated with PD098059).